Arch. Metall. Mater. **69** (2024), 2, 571-577

DOI: https://doi.org/10.24425/amm.2024.149785

UNISSA NICHUL[1], PANKAJ TAMBE[2], VIJAY HIWARKAR[1*]

ELECTROCHEMICAL BEHAVIOUR OF TEXTURED BETA C TITANIUM ALLOY IN 3.5% NaCl SOLUTION

The corrosion behaviour of a thermo-mechanically treated Beta C titanium alloy in a 3.5 wt% NaCl solution was investigated in this study. Thermomechanical processing prejudges titanium alloys to improve corrosion properties. Scanning electron microscopy and electron-backscattered diffractions were used to investigate the microstructural evolution and grain orientation after thermo-mechanical processing. The electrochemical characteristics of Beta C titanium alloy were examined using electrochemical impedance spectroscopy (EIS), corrosion potential, and corrosion current density measurements. The 45 percent deformed specimen experiences significant plastic deformation with increased dislocation density, resulting in strong ND //<111> orientation. However, the annealing after deformation exhibits a strong g-fiber texture with the lowest in-grain misorientation, which contributes to improving the corrosion resistance of the titanium alloy.

Keywords: Beta C; titanium alloy; EBSD; corrosion; microstructure

1. Introduction

Beta titanium and its alloys are growing ever more crucial from both an ecological and economic standpoint [1,2]. They have a high strength-to-weight ratio, formability, and high corrosion resistance and have been widely used in a broad range of applications ranging from the maritime to the chemical sector, all of which have benefited from titanium's exceptional mechanical as well as electrochemical properties [3-6]. Amongst all beta titanium alloy, Ti-3Al-8V-6Cr-4Mo-4Zr (Beta C) titanium alloy have been proposed for use in drill pipe, casing, tubing, pipeline, offshore vessels, and fasteners [7,8]. Each material must go through thermomechanical processing to be developed into a product. This alloy can obtain a wide range of mechanical and microstructural properties by altering the processing plan and subsequent thermal treatment. The titanium alloy Beta C is a well-known forgeable material [9,10]. Understanding crystallographic grain orientation following deformation and subsequent annealing is a critical characteristic to orient the various material properties. Beta C titanium alloy bears both (111) and (100) oriented grains, where, the former one holds higher surface energy than the latter one [11,12]. In the marine environment, titanium has the potential to swiftly produce a compact, stable, inert protective oxide coating, TiO_2 [8,12]. Given the long-term exposure of ships to seawater (sodium chloride), including their lengthy voyage, several alterations occur quickly and spontaneously on the metal surface. Previously, the oxide layers on titanium surfaces were described using a variety of approaches, each of which related to different external responses [4,6]. Numerous investigations have been carried out to understand the behaviour of Ti6Al4V alloy and pure titanium in NaCl solution [13-20]. The phase stability, microstructural evolution, corrosion process, and mechanical properties are well elucidated for these alloys. Efforts to employ beta-titanium alloys for marine applications have increased in recent years. The oxide film of beta-titanium alloys has primarily been studied empirically [21]. These include examinations into alloy chemical sciences, the utilization of multiple electrolytes, the atmosphere, temperature, and type of alloy. As part of practical application, thermomechanically driven corrosion studies have an effect on the material's durability in a certain niche. Electrochemical impedance spectroscopy (EIS), corrosion potential, and corrosion current density measurements are used to investigate the electrochemical properties of Beta C titanium alloy exposed to salt water. Furthermore, the efforts to comprehend the relationship between the corrosion behaviour of Beta C titanium alloys and microstructural evolutions such as grain orientations and grain size are unprecedented.

[1] DEFENCE INSTITUTE OF ADVANCED TECHNOLOGY, DEPARTMENT OF METALLURGICAL AND MATERIALS ENGINEERING, PUNE, MAHARASHTRA, INDIA
[2] VIT-AP UNIVERSITY, SCHOOL OF MECHANICAL ENGINEERING, AMARAVATI, ANDHRA PRADESH, INDIA

* Corresponding author: vijayhiwarkar@gmail.com

2. Materials and method

A extrudate and annealed solid bar of beta titanium alloy (Beta C^{TM}) was used in the present investigation. The chemical compositions of Beta C titanium alloy are 72.94 wt.% Ti, 3.60 wt.% Al, 7.61 wt.% V, 5.90 wt.% Cr, 5.25 wt.% Zr, 4.60 wt.% Mo [22]. The cylindrical specimens were wire-cut in size measuring 10 mm × 15 mm. In this study, three distinct specimens were used such as as-received, deformed, and annealed specimens. Metallographic polishing was done after wire-cut using emery paper including 400, 800, 1000, 1500, and 2000 grit followed by a mirror finish with alumina suspension. The deformed specimen was prepared by the uniaxial compression test (5980 series, Instron, UK) with a thickness reduction of up to 45%. Further, the 45% deformed specimen was annealed using a tubular furnace at 800°C for 2 hours in an argon atmosphere followed by water quenching, which is referred to as annealed specimen.

The X-ray diffraction (XRD) patterns were measured with a PANalytical XPert Pro Basic X-ray diffractometer unit using CuKα radiation with a wavelength of 0.15 nm at a scanning speed of 0.15 °/s to acquaint with the phases present in the processed titanium alloy. Hardness tests were carried out on the plane perpendicular to the deformation direction using a micro-hardness tester (Make-Matsuzawa, and model MMT-X7, Japan) using Vickers scale (HV) for 10 s dwell time and at 300 grams of load. The microstructures of all the specimens were observed using SIGMA, Carl Zeiss Field Emission Scanning Electron Microscopy (FESEM). FEI^{TM} Quanta-3d field emission gun (FEG) SEM equipped with a TSL-EDAX™ EBSD detector was employed for electron backscattered diffraction (EBSD). EBSD scans for all the specimens were taken with 20 kV voltage, 300 µm × 300 µm scan area, and 50 nm step size on a plane perpendicular to the deformation direction with identical beam conditions. Qualitative (Inverse pole figure (IPF), image quality (IQ) map), and quantitative analysis were done using EBSD techniques and were mapped with the confidence index (CI ≥ 0.1) to remove measurement uncertainty points. The corrosion resistance of the as-received (AR), deformed, and annealed Beta C titanium alloy was investigated in 3.5% NaCl (wt.%) made up of deionized water. The pH of the electrolyte was 7.1 using Hanna Instruments USA. In the present study, 3.5 wt.% NaCl is used as electrolyte [23]. An electrochemical setup (CH Instrument, Austin, TX, USA) was used to record electrochemical measurements according to the Meyer principle [24]. The electrochemical setup consists of a single-compartment glass cell with provided position to insert different standard electrode configurations, i.e., (a) reference electrode (SCE) (Hg/Hg_2Cl_2, 3M KCL), (b) counter electrode (CE) as the platinum electrode, and (c) working electrode (specimen) and a thermometer. The whole setup was fitted to potentiostat assembly. In the glass container, 250 ml of 3.5 wt.% NaCl was taken as an electrolyte. A long copper wire was soldered to the specimen's back keeping only one surface with an area of 0.785 cm^2 exposed to the NaCl solution. The specimens were polished using a series of SiC papers up to 2500 grits followed by a cloth finishing. Surface impurities and dirt were removed by ultrasonication using distilled water for 20 minutes. Open circuit potential (OCP) was performed for 2 hours with a scanning rate of 0.05 mV/s. Potentiodynamic polarization measurements were acquired in the potential range of ±2000 mV. The corrosion current density (i_{corr}) was calculated using Tafel plots. AC impedance spectrum for the specimens was extracted at the open-circuit potential with a scan frequency of 0.01 Hz to 100 kHz with an amplitude of 10 mV (rms). An optical microscope was used to evaluate the surface morphology using DMi8, Leica, Germany.

3. Results and discussion

3.1. X-ray diffraction

Fig. 1 depicts the XRD spectrum for as-received (AR), deformed, and annealed materials. The peaks revealed that the Beta C alloy displayed a mostly beta phase under all processing settings. The intensities (110) diffracting line were nearly the same for each condition; however, differences are noticeable in the $(200)_\beta$ and $(211)_\beta$ peaks. Broad peaks are visible for $(200)_\beta$ and $(211)_\beta$ diffracting lines after deformation due to the accumulation of dislocations and subsequently rise in microstrain [25]. The annealed specimen peaks appear narrower than the other two. After thermal treatment, dislocation annihilation produced a small peak.

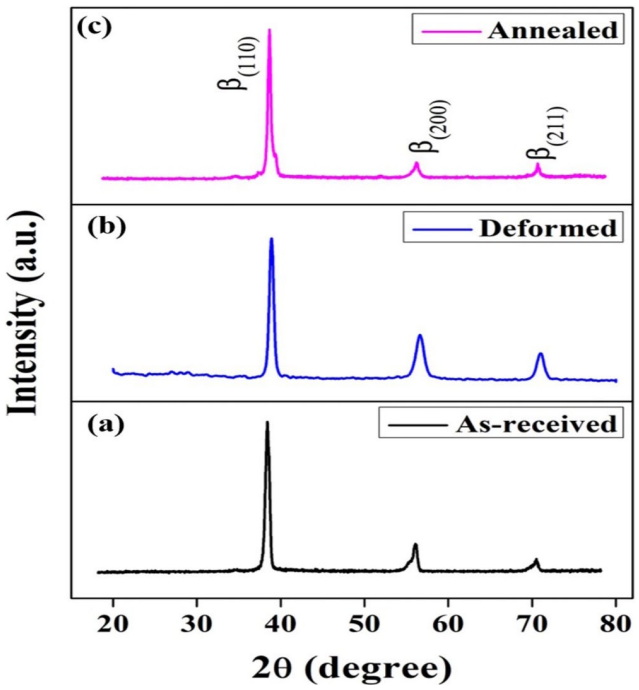

Fig. 1. XRD scans of as-received, deformed, and annealed Beta C titanium alloy

3.2. Microhardness

The changes in hardness in different conditions are shown in Fig. 2. Hardness of the as-received specimen is 279 HV.

A certain amount of the energy remains trapped as defects (dislocations) during deformation and the proportion of dislocation density increases amid higher deformation. [26,27]. The hardness value improved to 353 HV due to work hardening after 45% deformation. Annealing is essential for reducing internal stresses. As a result, as the temperature rises, the internal stresses decreases, and the overall number of dislocations decreases. The hardness decreases and reaches 300 HV after annealing.

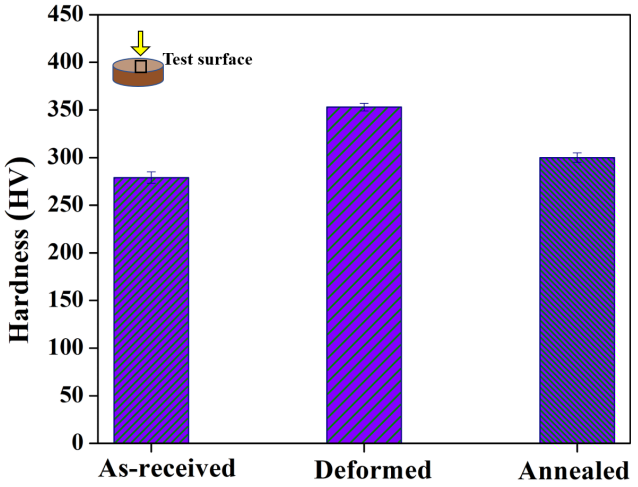

Fig. 2. Hardness values of as-received, deformed, and annealed Beta C titanium alloy

3.3. Microstructural analysis

Fig. 3(a-c) depicts representative FESEM micrographs obtained for several specimens. The initial microstructure of the as-received specimen suggests that equiaxed beta grains have a diameter of about 15 m. After 45% deformation, significant shear localizations with micro bands within a few grains were found. Grains alter shape by extending their grain boundaries due to higher deformation [28]. In the current study, the grains elongate and resemble pancake formations, with only a few deformed grains visible. After annealing, the microstructure is completely equiaxed, strain-free, and homogeneous. There are no noticeable microbands. Both qualitative and quantitative measurements were taken using EBSD measurement instruments for detailed microstructural examination. Inverse pole figure (IPF) maps of as-received, deformed, and annealed specimens are shown in Fig. 4 to understand the orientation of grains. The IPF maps were scanned with CI ≥ 0.1 indexing for Kikuchi patterns. In Fig. 4(a), the microstructure shows random orientation with ND//< 110 >, and ND//< 100 > oriented grains in the as-received specimen. The micrograph indicates the equiaxed beta grains with majority of ND// < 110 > oriented grains.

After 45% deformation, most of the grains appear distorted and fragmented which can be confirmed from Fig. 3(b). After deformation, a strong g-fiber was observed in Fig. 4(b). Strong ND// <111 > grains developed in significant numbers, and the proportion of ND// <100 > orientated grains increased in compared to the as-received specimen. Recrystallized grains are seen in Fig. 4(c), although they are coarser than the previous ones. And the orientation characteristics of the annealed specimen looked to be similar to the orientation characteristics of the deformed specimen (ND// <111 > or ND// <100 > grains). The darker portions in the microstructure are distorted zones with significant dislocation density, resulting in less indexed regions. For quantitative analysis, the misorientation angle in the beta titanium specimens is characterized by grain boundary length that is (a) low angle grain boundaries range 0-15°, and (b) high angle grain boundaries range 15-65°. The AR specimen has noticeable boundary length in both low and high-angle boundaries, as listed in TABLE 1. However, the deformed specimen exhibits the maximum length of the high angle grain boundary, demonstrates grain deforms significantly during the deformation.

TABLE 1

High angle and low angle boundary length of as-received, deformed, and annealed Beta C titanium alloy

Rotation Angle (°)		Boundary Length		
Minimum	Maximum	As-received	Deformed	Annealed
15	65	1.88 cm	22.93 cm	388 mm
0	15	0.5 cm	143.9 mm	551 µm

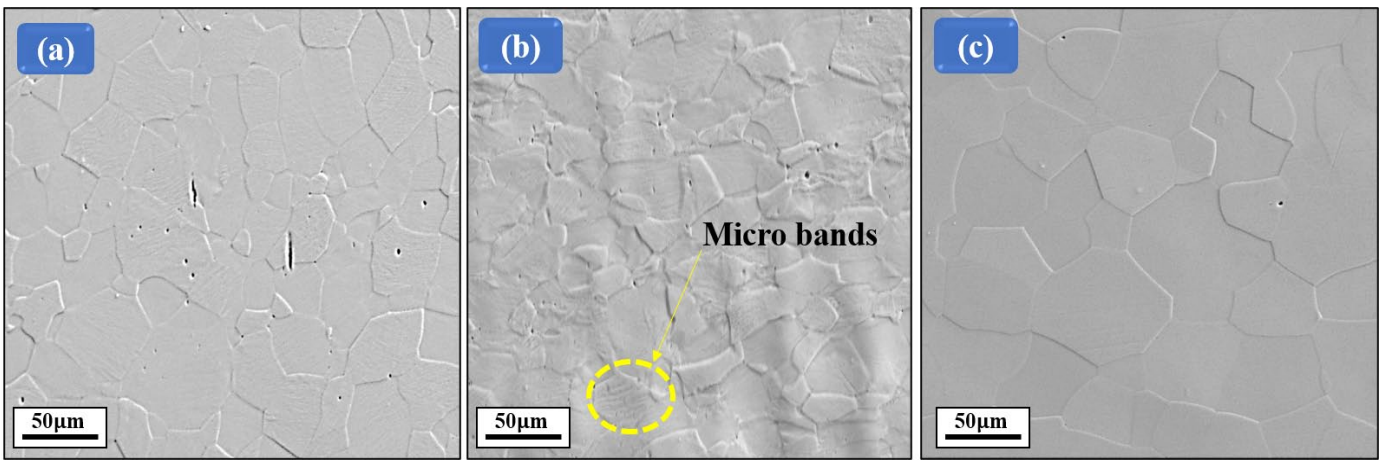

Fig. 3. FESEM image of (a) as-received, (b) deformed, and (c) annealed Beta C titanium alloy

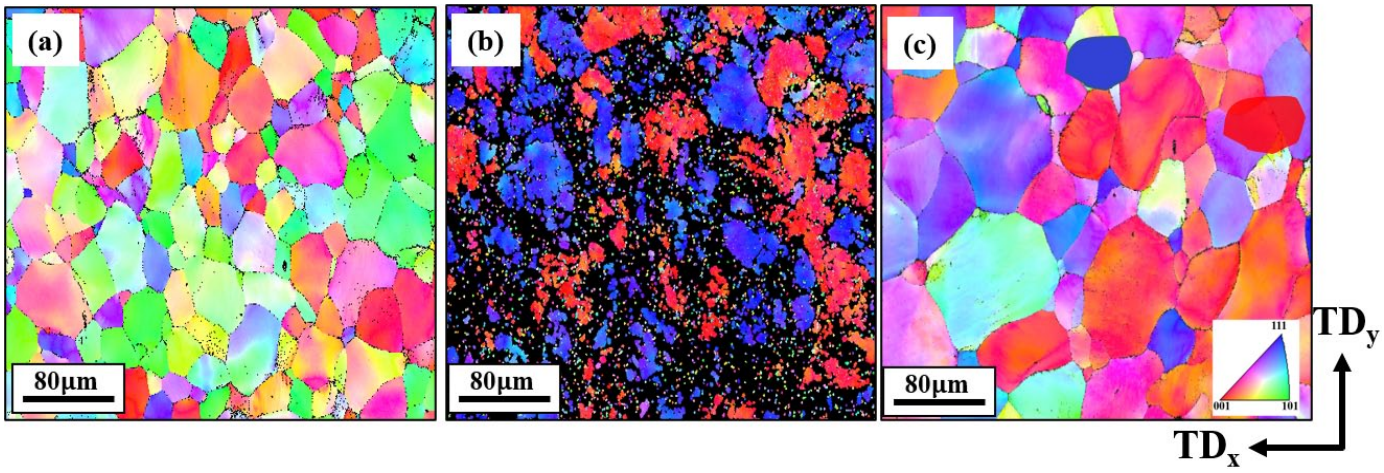

Fig. 4. Inverse pole figures of (a) as-received, (b) deformed, and (c) annealed titanium alloy

The severe deformation distorts the coarser grains into finer one, and sometimes grains elongated or flatten led to large grain boundary length. In compared to the other two specimens, the annealed specimen has a much shorter boundary length for both low and high-angle boundaries.

3.4. Corrosion study

The open-circuit potential (OCP) of as-received, deformed, and annealed specimens in 3.5 wt.% NaCl has been shown with time in Fig. 5(a). The initial potential (E_{ocp}) of the as-received specimen was +11 mV (SCE). Later, the potential (E_{ocp}) of the drop-down to –3 mV (SCE) at 1003 s and became stable at that potential. A sharp state transition was observed for the deformed specimen with the initial potential of –633 mV (SCE) at 0 s, then the curve moved upward and straighten at 3205 s with a potential of –42 mV (SCE). A hyperbolic curve pointing downward implies that corrosion attack has accelerated near the distorted region.

The mobile region allows the electrolyte to enter the surface and change the oxide layer. The annealed specimens have superior corrosion resistance than the other two because the profile reaches stability at +43 mV (SCE). The displacement of curves in a positive direction leads to passive film formation [29]. Despite the corrosive nature of the NaCl solution, the annealed specimens' curves stepped up higher (towards the positive direction), demonstrating film stability. The potentiodynamic polarisation curves of the as-received, deformed, and annealed specimens are shown in Fig. 5(b). The corrosion potential (E_{corr}), corrosion current density (i_{corr}), and corrosion rate were calculated and tabulated in TABLE 2. The average corrosion potentials (E_{corr}) estimated from the linear polarization curve were –507 mV (SCE), –889 mV (SCE), and –474 mV (SCE) for as-received, deformed, and annealed specimens. The curve of the as-received specimen position at corrosion current density (i_{corr}) of 8.9 µA/cm^2 and a corrosion potential of –507 mV (SCE). The curve of the deformed specimen shift towards negative potential with higher i_{corr} values (13.1 µA/cm^2) in comparison to the as-received specimen. Curves altered in a positive direction promote the growth of the passive film, whereas curves shifted in a negative direction indicate oxide film disintegration or no oxide production of the film [29,30]. Even a minor deformation allows the NaCl electrolyte to enter the metal surface and cause

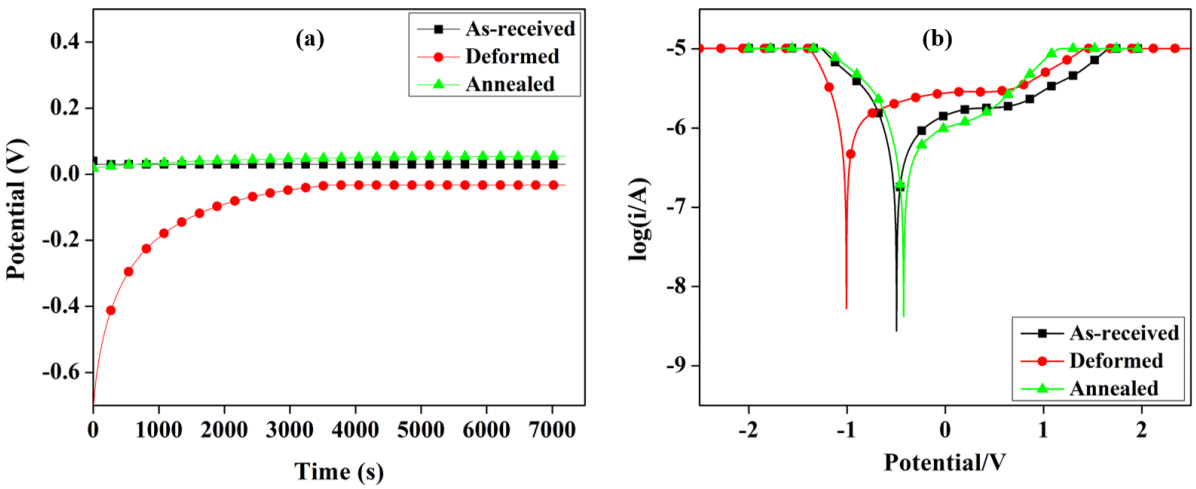

Fig. 5. (a) Open circuit potential, and (b) Tafel plot of as-received, deformed, and annealed Beta C titanium alloy

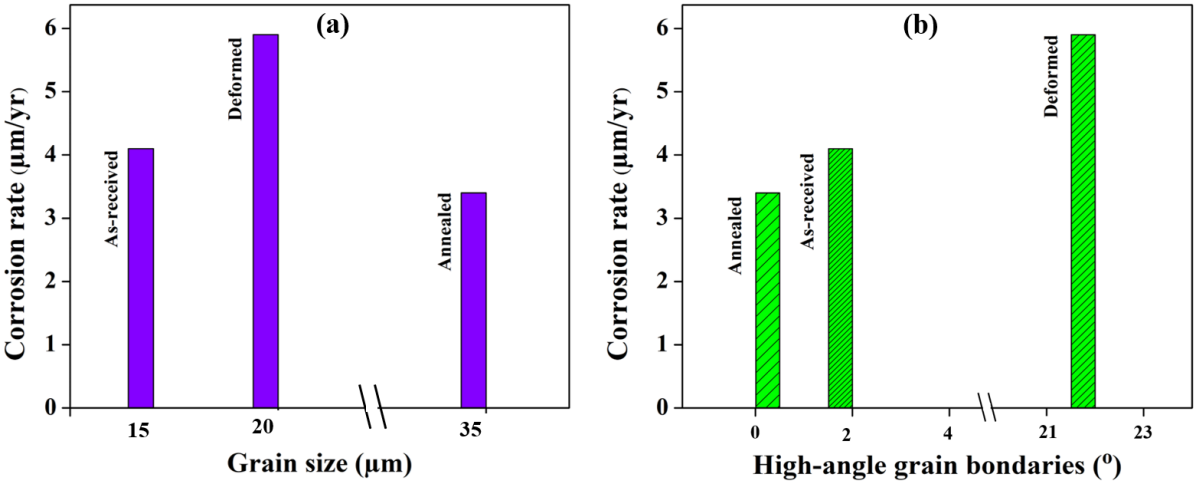

Fig. 6. (a) Corrosion rate vs grain size, and (b) corrosion rate vs high-angle grain boundaries of titanium alloys

changes in the oxide film. As a result, the annealed specimen's curve trends to the extreme right, indicating the presence of the protective oxide layer.

TABLE 2

Electrochemical parameters of titanium specimens Tafel extrapolation

Specimens	E_{corr} (mV)	i_{corr} (µA/cm^2)	Corrosion rate (mm/yr)
As-received	–507 ± 5.8	10.3 ± 0.7	0.055
Deformed	–889 ± 11	16.6 ± 1.9	0.089
Annealed	–474 ± 6.2	9.23 ± 1.3	0.049

Fig. 6 depicts the change of corrosion characteristics in relation to thermomechanical processing and microstructural evolution. Fig. 6(a) depicts the relationship of corrosion rate with respect to grain size for each specimen in NaCl solution. As expected, rising temperatures reduce the confined free energy or strained zone, causing larger grains to form [31]. Good corrosion resistance is observed for larger grain size and lower i_{corr} values. Fig. 6(b) displays the plot of corrosion rate versus high-angle grain boundary length. This implies that the annealed specimen with the lowest grain boundary length (388 mm) had the lowest corrosion rate. It has been demonstrated that decreasing grain boundary length and increasing grain size lower corrosion rate. The metal-oxide layer-electrolyte interface response was studied using electrochemical impedance spectroscopy. The Nyquist diagrams of as-received, deformed, and annealed specimens are shown in Fig. 7.

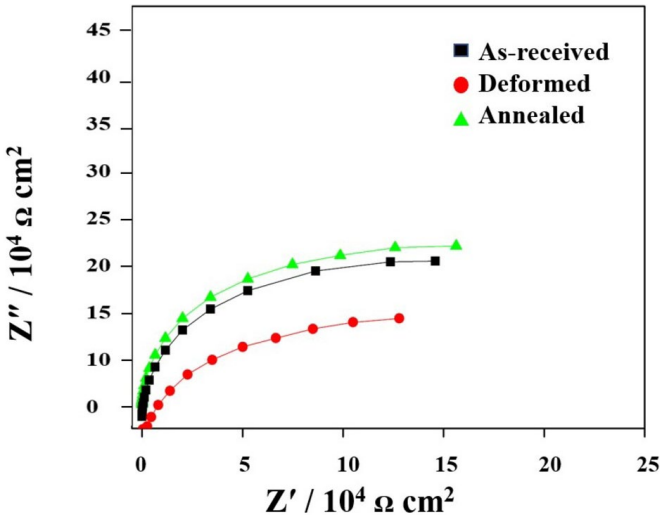

Fig. 7. Nyquist plot of as-received, deformed, and annealed specimen

The as-received specimen shows a characteristic single capacitive loop. An oxide layer provides a lower resistance to electrolytes affecting the surface, indicating the curve of the deformed specimen shrinks significantly.

As a result, with aggressive electrolytes, the specimen's impedance will be significantly lowered. However, the annealed specimen had a larger capacitive loop than the other two. Although there is no discernible difference at the lowest frequency, the impedance curve varies dramatically at higher frequencies. Fig. 8 depicts the surface morphology of a post-electrochemical test specimen as received, distorted, and annealed. The as-received and annealed microstructures show no traces or flaws. However, the deformed specimen micrograph appears a little darker in shade. For the development of products, the materials typically endure thermo-mechanical processing which comprises deformation and annealing. During deformation, the product acquires a desired shape that is accompanied by internal and surface stresses. Therefore, based on the findings, the use of annealed specimens with better surface properties is more appropriate in marine applications.

4. Conclusion

The present study was carried out to understand the electrochemical response of Beta C titanium alloy (under different conditions) upon exposure to 3.5 wt.% NaCl solution. The following are the main findings:

1. The annealed specimen's grain boundary length was found to be noticeably different (by roughly two times) from the

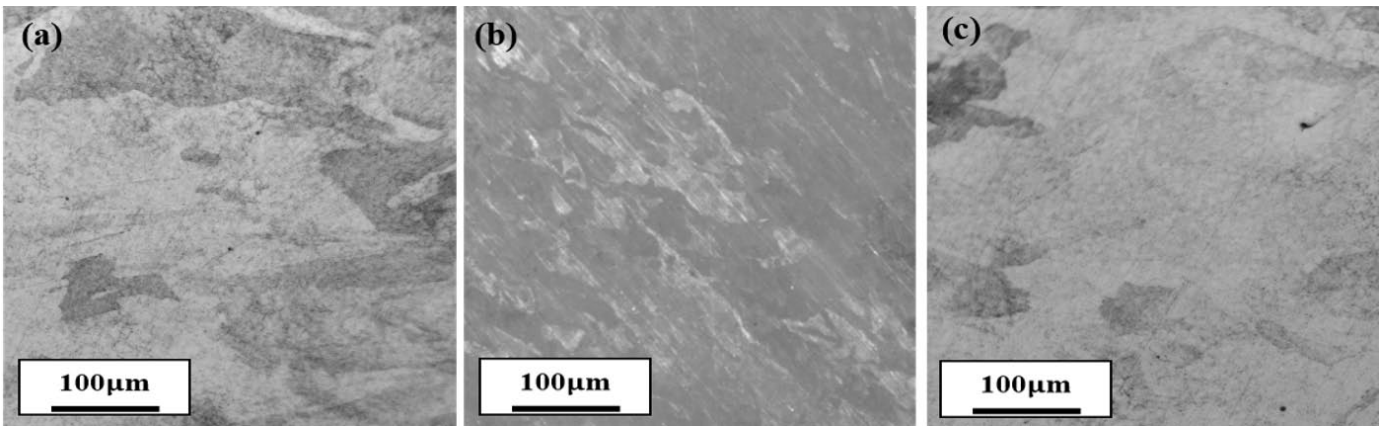

Fig. 8. Optical micrographs of as-received, deformed, and annealed Beta C titanium alloy

as-received specimen, which is thought to be an important factor in improving corrosion resistance.

2. Following heat treatment, the surface property improved, with the corrosion rate being lowest for annealed specimens and highest for deformed specimens.
3. In contrast to the other two, the annealed specimen bears a protective passive layer. The corrosion potential of deformed specimens was observed to be lowest with higher corrosion current density, suggesting a weak oxide film compared to the annealed specimen. Annealed Beta C titanium alloy holds suitable performing capabilities for marine applications.

Acknowledgment

Authors would like to acknowledge the OIM Laboratory, IIT Bombay for their technical support.

REFERENCES

[1] J. Gao, Y. Huang, D. Guan, A.J. Knowles, L. Ma, D. Dye, W.M. Rainforth, Deformation mechanisms in a metastable beta titanium twinning induced plasticity alloy with high yield strength and high strain hardening rate. Acta Mater. **152**, 301-314 (2018). DOI: https://doi.org/10.1016/j.actamat.2018.04.035

[2] Y. Li, J. Xu, Is niobium more corrosion-resistant than commercially pure titanium in fluoride-containing artificial saliva? Electrochim. Acta. **233**, 151-166 (2017). DOI: https://doi.org/10.1016/j.electacta.2017.03.015

[3] Y. Yang, P. Castany, M. Cornen, I. Thibon, F. Prima, T. Gloriant, Texture investigation of the superelastic Ti-24Nb-4Zr-8Sn alloy. J. Alloys Compd. **591**, 85-90(2014). DOI: https://doi.org/10.1016/j.jallcom.2013.12.207

[4] J. Li, Y. Bai, Z. Fan, S. Li, Y. Hao, R. Yang, Y. Gao, Effect of fluoride on the corrosion behavior of nanostructured Ti-24Nb-4Zr-8Sn alloy in acidulated artificial saliva, J. Mater. Sci. Technol. **34**, 1660-1670 (2018). DOI: https://doi.org/10.1016/j.jmst.2018.01.008

[5] C. Lan, Y. Wu, L. Guo, F. Chen, Effects of cold rolling on microstructure, texture evolution and mechanical properties of Ti-32.5Nb-6.8Zr-2.7Sn-0.3O alloy for biomedical applications. Mater. Sci. Eng. A. **690**, 170-176 (2017). DOI: https://doi.org/10.1016/j.msea.2017.02.045

[6] I. Çaha, A.C. Alves, P.A.B. Kuroda, C.R. Grandini, A.M.P. Pinto, L.A. Rocha, F. Toptan, Degradation behavior of Ti-Nb alloys: Corrosion behavior through 21 days of immersion and tribocorrosion behavior against alumina, Corros. Sci. **167**, 108488 (2020). DOI: https://doi.org/10.1016/j.corsci.2020.108488

[7] R.A. Antunes, C.A.F. Salvador, M.C.L. de Oliveira, M.C.L. de Oliveiraa, C.A.F. Salvador, Materials selection of optimized titanium alloys for aircraft applications. Mater. Res. 21 (2018). DOI: https://doi.org/10.1590/1980-5373-mr-2017-0979

[8] J. Pang, D.J. Blackwood, Corrosion of titanium alloys in high temperature near anaerobic seawater, Corros. Sci. **105**, 17-24. (2016). DOI: https://doi.org/10.1016/j.corsci.2015.12.011

[9] J. Krawczyk, Ł. Frocisz, R. Dąbrowski, E. Rozniata, T. Śleboda, The range of the occurrence of α phase in near β titanium alloys. Key Eng. Mater. **682**, 77-82. (2016). DOI: https://doi.org/10.4028/www.scientific.net/KEM.682.77

[10] U. Nichul, R. Khatirkar, A. Dhole, V. Hiwarkar, Cold compression behavior on the evolution of microstructure and texture in Beta C titanium alloy. J. Alloys Compd. **887**, 161400 (2021). DOI: https://doi.org/10.1016/j.jallcom.2021.161400

[11] N.P. Gurao, G. Manivasagam, P. Govindaraj, R. Asokamani, S. Suwas, Effect of Texture and Grain Size on Bio-Corrosion Response of Ultrafine-Grained Titanium. Metall. Mater. Trans. A. **44** (2013) 5602-5610. DOI: https://doi.org/10.1007/s11661-013-1910-9

[12] U. Nichul, V. Hiwarkar, Carbon dot complimentary green corrosion inhibitor for crystallographically textured Beta C titanium alloy for marine application : A state of art. J. Alloys Compd. **962**, 171116 (2023). DOI: https://doi.org/10.1016/j.jallcom.2023.171116

[13] J. Lu, W. Zhang, W. Huo, Y. Zhao, W. Cui, Y. Zhang, Electrochemical corrosion behavior and mechanical properties of nanocrystalline Ti-6Al-4V Alloy induced by sliding friction treatment. Materials (Basel). 12 (2019). DOI: https://doi.org/10.3390/ma12050760.

[14] J. Jin, S. Zhou, W. Zhang, K. Li, Y. Liu, D. Chen, L.-C. Zhang, Effect of ceramic types on the microstructure and corrosion be-

havior of titanium matrix composites produced by selective laser melting. J. Alloys Compd. **918**, 165704 (2022).
DOI: https://doi.org/10.1016/j.jallcom.2022.165704

[15] X. Yang, X. Dong, W. Li, W. Feng, Y. Xu, Effect of solution and aging treatments on corrosion performance of laser solid formed Ti-6Al-4V alloy in a 3.5 wt.% NaCl solution. J. Mater. Res. Technol. **9**, 1559-1568 (2020).
DOI: https://doi.org/10.1016/j.jmrt.2019.11.082

[16] H.S. Abdo, E.S.M. Sherif, H.A. El-Serehy, Manufacturing of ti-6%al and ti-6%al-4%v alloys and their corrosion in sodium chloride solutions. Crystals. **10**, 9-11 (2020).
DOI: https://doi.org/10.3390/cryst10030181

[17] S. Gudić, L. Vrsalović, D. Kvrgić, A. Nagode, Electrochemical Behaviour of Ti and Ti-6Al-4V Alloy in Phosphate Buffered Saline Solution. Materials (Basel). **14**, 7495 (2021).
DOI: https://doi.org/10.3390/ma14247495

[18] J. Jaquez-Muñoz, C. Gaona-Tiburcio, A. Lira-Martinez, P. Zambrano-Robledo, E. Maldonado-Bandala, O. Samaniego-Gamez, D. Nieves-Mendoza, J. Olguin-Coca, F. Estupiñan-Lopez, F. Almeraya-Calderon, Susceptibility to Pitting Corrosion of Ti-CP2, Ti-6Al-2Sn-4Zr-2Mo, and Ti-6Al-4V Alloys for Aeronautical Applications. Metals (Basel). **11**, 1002 (2021).
DOI: https://doi.org/10.3390/met11071002

[19] R.N. Elshaer, K.M. Ibrahim, Study of Microstructure, Mechanical Properties, and Corrosion Behavior of As-Cast Ni-Ti and Ti-6Al-4V Alloys. J. Mater. Eng. Perform. **32**, 7831-7845 (2022).
DOI: https://doi.org/10.1007/s11665-022-07654-y

[20] R. Li, L. Liu, Y. Cui, R. Liu, F. Wang, Corrosion behavior of pure Ti under continuous NaCl solution spraying at 600°C. Npj Mater. Degrad. **6**, 53 (2022).
DOI: https://doi.org/10.1038/s41529-022-00257-x

[21] J. Affi, Gunawarman, Y. Yetri, H. Fajri, D. Juliadmi, N.F. Nuswantoro, Nurbaiti, S. Fonna, D.H. Tjong, M. Manjas, Corrosion Resistance of β type titanium (TNTZ) in 3%NaCl solution. IOP Conf. Ser. Mater. Sci. Eng. 602 (2019).
DOI: https://doi.org/10.1088/1757-899X/602/1/012070

[22] C. Madikizela, L.A. Cornish, L.H. Chown, H. Möller, Microstructure and mechanical properties of selective laser melted Ti-3Al-8V-6Cr-4Zr-4Mo compared to Ti-6Al-4V. Mater. Sci. Eng. A. **747**, 225-231 (2019).
DOI: https://doi.org/10.1016/j.msea.2018.12.100

[23] G. Yang, L. Ying, L. Haichao, Experimental studies on the local corrosion of low alloy steels in 3.5% NaCl. Corros. Sci. **43**, 397-411 (2001).
DOI: https://doi.org/10.1016/S0010-938X(00)00090-1

[24] J.-M. Meyer, Corrosion resistance of nickel-chromium dental casting alloys. Corros. Sci. **17**, 971-982 (1977).
DOI: https://doi.org/10.1016/S0010-938X(77)80012-7

[25] O. Muránsky, L. Balogh, M. Tran, C.J. Hamelin, J.S. Park, M.R. Daymond, On the measurement of dislocations and dislocation substructures using EBSD and HRSD techniques. Acta Mater. **175**, 297-313 (2019).
DOI: https://doi.org/10.1016/j.actamat.2019.05.036

[26] A.L. Etter, M.H. Mathon, T. Baudin, V. Branger, R. Penelle, Influence of the cold rolled reduction on the stored energy and the recrystallization texture in a Fe-53%Ni alloy. Scr. Mater. (2002).
DOI: https://doi.org/10.1016/S1359-6462(01)01245-3

[27] C. Deng, S.F. Liu, X.B. Hao, J.L. Ji, Z.Q. Zhang, Q. Liu, Orientation dependence of stored energy release and microstructure evolution in cold rolled tantalum. Int. J. Refract. Met. Hard Mater. **46**, 24-29 (2014).
DOI: https://doi.org/10.1016/j.ijrmhm.2014.05.005

[28] A. Gupta, R.K. Khatirkar, T. Dandekar, J.S. Jha, S. Mishra, Recrystallization behavior of a cold rolled Ti–15V–3Sn–3Cr–3Al alloy. J. Mater. Res. **34**, 3082-3092 (2019).
DOI: https://doi.org/10.1557/jmr.2019.225

[29] R. Chelariu, G. Bolat, J. Izquierdo, D. Mareci, D.M. Gordin, T. Gloriant, R.M. Souto, Metastable beta Ti-Nb-Mo alloys with improved corrosion resistance in saline solution. Electrochim. Acta. **137**, 280-289 (2014).
DOI: https://doi.org/10.1016/j.electacta.2014.06.021

[30] I. Milošev, G. Žerjav, J.M. Calderon Moreno, M. Popa, Electrochemical properties, chemical composition and thickness of passive film formed on novel Ti–20Nb–10Zr–5Ta alloy. Electrochim. Acta. **99**, 176-189 (2013).
DOI: https://doi.org/10.1016/j.electacta.2013.03.086

[31] U. Nichul, V. Kumar, V. Hiwarkar, Electrochemical performance of heat-treated beta titanium alloy in artificial saliva: Key role of grain size. Mater. Today Commun. **37**, 106981 (2023).
DOI: https://doi.org/10.1016/j.mtcomm.2023.106981